J. Phys. Chem. A
October 17, 2013

The Collision Efficiency of Water in the Unimolecular Reaction CH_4 (+ H_2O) ⇆ CH_3 + H (+ H_2O): One-Dimensional and Two-Dimensional Solutions of the Low-Pressure-Limit Master Equation

Ahren W. Jasper,[a,]* James A. Miller,[b] and Stephen J. Klippenstein[b]

[a]*Combustion Research Facility, Sandia National Laboratories, PO Box 969, Livermore, CA 94551-0969, USA*
[b]*Chemical Sciences and Engineering Division, Argonne National Laboratory, Argonne, IL 60439, USA*

Abstract

The low-pressure-limit unimolecular decomposition of methane, CH_4 (+ M) ⇆ CH_3 + H (+ M), is characterized via low-order moments of the total energy, E, and angular momentum, J, transferred due to collisions. The low-order moments are calculated using ensembles of classical trajectories, with new direct dynamics results for M = H_2O and new results for M = O_2 compared with previous results for several typical atomic (M = He, Ne, Ar, Kr) and diatomic (M = H_2 and N_2) bath gases and one polyatomic bath gas, M = CH_4. The calculated moments are used to parameterize three different models of the energy transfer function, from which low-pressure-limit rate coefficients for dissociation, k_0, are calculated. Both one-dimensional and two-dimensional collisional energy transfer models are considered. The collision efficiency for M = H_2O relative to the other bath gases (defined as the ratio of low-pressure limit rate coefficients) is found to depend on temperature, with, e.g., $k_0(H_2O)/k_0(Ar)$ = 7 at 2000 K but only 3 at 300 K. We also consider the *rotational* collision efficiency of the various baths. Water is the only bath gas found to fully equilibrate rotations, and only at temperatures below 1000 K. At elevated temperatures, the kinetic effect of "weak-collider-in-J" collisions is found to be small. At room temperature, however, the use of an explicitly two-dimensional master equation model that includes weak-collider-in-J effects predicts smaller rate coefficients by 50% relative to the use of a statistical model for rotations. The accuracies of several methods for predicting relative collision efficiencies that do not require solving the master equation and that are based on the calculated low-order moments are tested. Troe's weak collider efficiency, β_c, includes the effect of saturation of collision outcomes above threshold and accurately predicts the relative collision efficiencies of the nine baths. Finally, a brief discussion is presented of mechanistic details of the energy transfer process, as inferred from the trajectories.

Keywords: Classical trajectory simulations, pressure dependence, kinetics, direct dynamics, weak collider

I. Introduction

Practical and accurate rate-coefficient calculations require generally-applicable and validated theoretical models for thermochemistry, intramolecular dynamics (the specific or microcanonical rate coefficients $k(E,J)$ associated with bond-breaking, isomerization, etc…), and collisional energy transfer.[1,2,3,4] The multifarious efforts of the last few decades developing electronic structure methods and codes,[5] along with new methods for treating vibrational anharmonicity,[6,7,8,9,10,11] now allow for routine predictions of thermochemistry with "chemical accuracy" for molecular systems.[12,13] Likewise, the continued development of transition state theory[14] (TST), including direct methods that couple with electronic structure calculations[15,16] and applications of TST to nontrivial reaction types,[17,18,19,20] allows for quantitative theoretical descriptions of intramolecular kinetics for many kinds of molecular systems.[21] Methods for predicting collisional energy transfer are much less well developed. In fact, collisional energy transfer is almost always treated empirically and with simple models in practical thermal chemical rate-coefficient calculations.[1,2,3,4]

While high-level dynamical calculations of collisional energy transfer (e.g., inelastic quantum scattering) may be carried out for small systems,[22] such calculations are prohibitively expensive for molecular systems with more than a few atoms. The high internal energies and long timescales involved in collisions relevant to thermal kinetics can preclude quantum scattering calculations even for small systems. Mixed quantum/classical methods[23,24] show promise of broadening the range of applicability of high-level calculations. Here we use classical trajectories[25,26,27,28,29,30,31] to predict collisional energy transfer dynamics relevant to low-pressure unimolecular reactions.[32,33,34,35,36] In addition to being a practical necessity for molecular systems, the present use of classical mechanics may be formally motivated as follows: Thermal low-pressure-limit unimolecular rate coefficients are likely to be most sensitive to low-order moments of the total energy and total angular momentum transferred into and out of highly rovibrationally excited states of the unimolecular reactant and not fine details (e.g., state-selected transition probabilities) of the collisions.[32,37] The expectation that these low-order moments are well described by classical mechanics may be justified via the Ehrenfest theorem[38] and semiclassical arguments,[39,40] although the quantitative validity of this assumption remains largely untested for the present kind of application.

We have previously used classical trajectories to characterize the collisional energy transfer involved in the low-pressure-limit and falloff rate coefficients for the reaction CH_4 (+ M) $\leftrightarrows$ CH_3 + H (+ M) in eight baths.[41,42] At room temperature, the collision efficiencies were found to be similar for all the baths considered except for Ne, which was relatively less efficient, and H_2 and CH_4, which were relatively more efficient colliders. Temperature dependence was observed, with the relative collision efficiencies of the lighter baths increasing more with temperature than those of the heavier baths. These results may be rationalized by noting that at lower temperatures, where the relative kinetic energies are comparable to the interaction energies, the strength of the target–bath interaction energy has some influence on the details of the collisions. At higher temperatures, the differences in well depths for the different baths are small compared to the relative kinetic energy, and the collision efficiencies are instead influenced more by the collision frequency and therefore the mass of the bath gas collider.

The results of the trajectory calculations were used to parameterize a single-exponential-down[1] master equation model for energy transfer with the "microcanonical strong-collider-in-*J*" model for angular momentum.[43,44] This model has been called the "*E*,*J*" model in past work, and it requires a single low-order moment of the collisional energy transfer function: the average energy transferred in deactivating collisions, $\alpha \equiv \langle \Delta E_\mathrm{d} \rangle$. Using values of $\langle \Delta E_\mathrm{d} \rangle$ obtained from the trajectory calculations and the *E*,*J* model, the resulting empirical-parameter-free pressure-dependent rate coefficients were found to agree with available experimental results to within a factor of two. The principal sources of error in these calculations may be identified as (1) the neglect of vibrational anharmonicity in the state counts and partition functions of CH_4 and (2) simplifications in the model for the energy transfer function.

Troe and Ushakov also carried out a detailed theoretical study of the CH_4 (+ M) $\leftrightarrows$ CH_3 + H (+ M) reaction.[45] Their treatment differed in several ways from our investigation. Notably, they explicitly included vibrational anharmonicity corrections, and they used a different model for pressure dependence. Their pressure dependent rate coefficients were found to be in very good agreement with available experimental kinetics, with an empirical energy transfer parameter just ~20% smaller than our calculated value. This difference is close to the expected statistical error in the trajectory calculation and in the fitted analytic representation given by us for α. Troe and Ushakov noted the lack of experimental and theoretical information regarding the collisional efficiencies of M = H_2O and O_2 in promoting methane dissociation. The principal goal of the present work is to extend our previous theoretical characterizations of collisional energy transfer in methane to include M = H_2O and O_2, two important colliders in combustion applications.

Water has been shown experimentally to be a much more efficient collider than typical atomic and diatomic baths. For example, water was found experimentally to be ~20 times more efficient than Ar in promoting H_2O decomposition[46] as well as the H + O_2 association reaction.[47] Notably, significant temperature dependence in the relative collision efficiencies of M = H_2O and Ar was reported in the former reaction but not in the latter reaction. Despite these and other systematic studies involving several bath gases,[26,27,48,49,50] the dependence of collisional energy transfer dynamics on temperature, bath gas, and chemical structure of the unimolecular reactant is not well understood. Another goal of the present study is to quantify some of these effects for water relative to typical atomic and diatomic baths for methane dissociation, as well as to validate the present potential energy surfaces and classical trajectory methods for studying these trends.

The potential energy surface is often a significant source of error in trajectory calculations of collisional energy transfer. Competing simplified functional forms have been tested against one another,[26,27,28,51,52,53,54] and it has been shown that predicted low-order moments depend most sensitively on the "softness" of the repulsive target–bath interaction but are not significantly affected by the intramolecular description of the target (i.e., the unimolecular reactant). We recently tested several analytical functional forms against full-dimensional direct dynamics trajectory calculations.[42] These comparisons showed that while typical simplified analytical functional forms could be reliably used to calculate low-order energy transfer moments for atomic baths, the use of a separable and pairwise description of the target–bath intermolecular interaction may introduce errors for systems with significantly anisotropic intermolecular potentials.

One may expect significant orientation-dependence in the CH_4 + H_2O interaction potential and for these anisotropies to be poorly described using simplified functional forms for the intermolecular potential energy surface. Here, we do not attempt to parameterize a specific interaction energy surface for CH_4 + H_2O. Instead, we validate a relatively inexpensive "scale all correlation" (SAC) variant of MP2 against higher-level interaction energies and use it to carry out direct trajectory calculations. While the use of direct dynamics with ab initio quantum chemistry methods remains rare in trajectory studies of energy transfer, here it allows for the full-dimensional anisotropic interaction potential to be realistically characterized. The significant tradeoff of the present approach, of course, is the increased computational cost, and we do not attempt to run the very large ensembles of trajectories required to elucidate fine details of energy transfer with good statistics.[31,51,55] Instead, we focus on calculating low-order moments of the total energy and total angular momentum transferred due to collisions, which can be usefully converged with relatively small ensembles. The present approach is designed to enable the use of high-level potential energy surfaces for characterizing energy transfer and for building practical models of non-reactive collisions.

Finally, the effect of angular momentum on the unimolecular kinetics of methane dissociation is considered and trends are identified for the different baths. The trajectory calculations in principle allow for the parameterization of detailed energy transfer models, and this work will be reported elsewhere.[56] Here we use the trajectory results to parameterize three simple energy transfer models that differ in their treatment of angular momentum: a one-dimensional exponential down model (1D), a two-dimensional exponential down and microcanonical strong-collider-in-*J* model (2D/φ), and an explicitly two-dimensional, two-exponential model (2D). The 1D model neglects angular momentum changes due to collisions. The 2D/φ model is the limit of the explicitly 2D model in which collisions are strong enough to statistically equilibrate *J* at fixed E. The relative accuracies of the 1D and 2D/φ models (which have been called the "*E*" and "*E,J*" models elsewhere) have been discussed previously,[44] and both models have been widely used. Explicitly 2D master equation calculations, on the other hand, are very rare.[57,58,59] Furthermore, here we consider the accuracy of various energy transfer functions with parameters calculated via classical trajectories, whereas past work involving the 1D, 2D/φ, and 2D models has almost exclusively involved empirically-adjusted parameters. While qualitative differences in the various models could be studied using such empirical parameters, the present methods allow for an assessment of the *predictive* accuracy of the various models, as well as an opportunity to quantify the kinetic effects of their different approximations. Here, we quantify the "weak-collider-in-*J*" effect by comparing the results of the 2D/φ and 2D models for CH_4 dissociation for several baths.

This paper is organized as follows. In Sec. II, details of the trajectory calculations and potential energy surfaces are presented, including validation calculations of the SAC potential energy surface for CH_4 + H_2O and a new separable pairwise parameterization for M = O_2. In Sec. III, several low-order moments of the total energy and total angular momentum transferred in CH_4 + M collisions are presented, and comparisons are made among the various baths. The low-pressure-limit rate coefficient for methane dissociation in several baths is calculated using the one-dimensional and two-dimensional master equation models discussed above. The quantitative effects of the different models' approximations are quantified and related to the efficiencies of the bath gas colliders in equilibrating rotations. The collision efficiency of water is evaluated relative to other baths by comparing low-pressure-limit rate coefficients. Several approximate methods for calculating relative collision efficiencies are compared with the solutions of the master equation and with Troe's weak collider correction, β_c. Finally, mechanistic details of collisional energy transfer for M = H_2O are compared with other baths; this includes a discussion of the cross section for collisional energy transfer and the likelihood of multiple collision encounters. Section V is a summary.

II. Theory

Potential energy surfaces. Direct dynamics trajectories for M = H_2O were carried out using a "scale all correlation" (SAC)[60] variant of MP2/aug-cc-pVDZ, with the SAC parameter optimized to $F = 1.25$. This value of F was optimized to best reproduce counterpoise corrected QCISD(T)/CBS interaction energies along six CH_4 + H_2O approaches, where the complete basis set limit (CBS) was estimated using a two-point formula and the aug-cc-pVDZ and aug-cc-pVTZ basis sets.

The QCISD(T)/CBS and SAC/aug-cc-pVDZ energies along the six approaches are compared in Fig. 1. In the three approaches in Fig. 1(a), the O atom of water is oriented toward CH_4 and approaches either a face, edge, or vertex of tetrahedral CH_4 at its classical equilibrium geometry. For this set of orientations, the vertex approach is lowest at greater distances relative to the other two approaches. In Fig. 1(b), a similar set of approaches is shown, but for water oriented with one of its H atoms pointed toward CH_4. Here, the vertex approach is only weakly bound at long range and is strongly repulsive at short distances, while the other two approaches have shorter-ranged repulsive walls and lower energies. The significant orientation dependence in these two sets of approaches is well reproduced by the SAC method. (We note again that these anisotropies may be difficult to include accurately in simple analytic functional forms.) For the five most attractive approaches, the SAC binding energies are within 15% of the higher-level values. The sixth approach is relatively more repulsive than the others, as predicted by both methods, although the SAC well depth is somewhat larger than the QCISD(T) value. Just as important for the present application, both methods predict repulsive walls with similar shapes and distances.

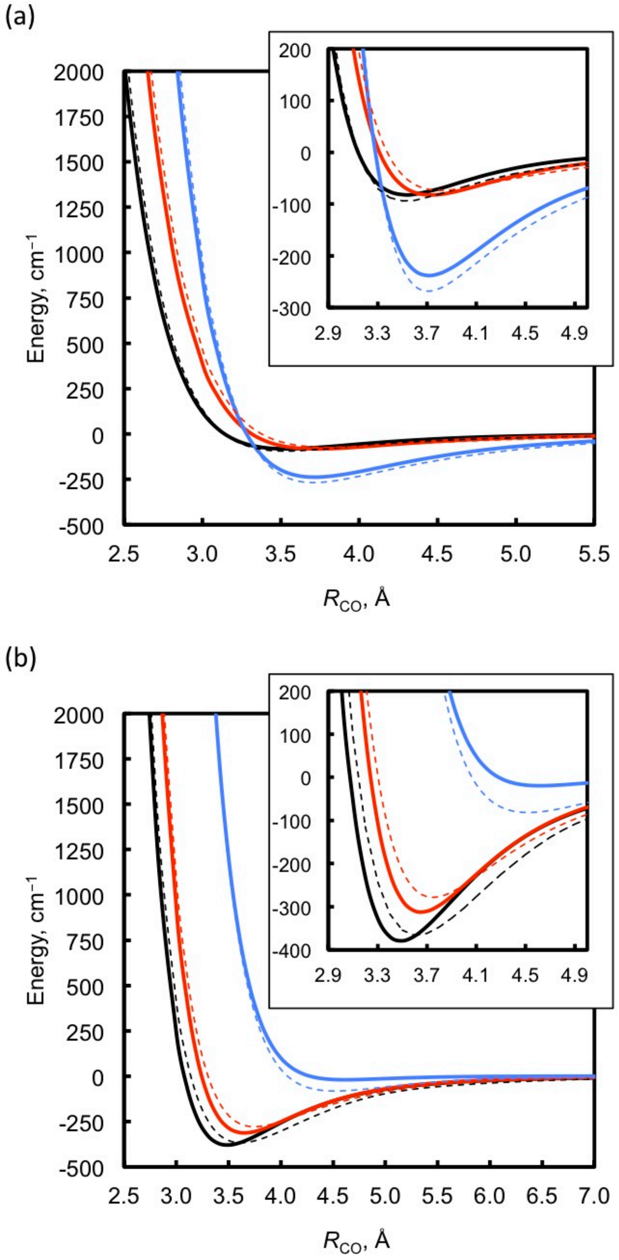

Figure 1. $CH_4 + H_2O$ interaction potential for face (black), edge (red), and vertex (blue) (a) "O-in" and (b) "H-in" approaches. The solid lines in all four panels are QCISD(T)/CBS energies, and the dashed lines are SAC/aug-cc-pVDZ energies. The insets highlight the van der Waals well.

For M = O_2, a new separable pairwise parameterization was obtained for CH_4 + O_2 using the same strategy as previously employed[42] for M = H_2, N_2, and CO. The intramolecular PES of CH_4 was described via the "tight binding" (TB) parameterization of Wang and Mak;[61] tight binding is an efficient semiempirical method that is sometimes called extended Hückel theory. The one-dimensional intramolecular PES for triplet O_2 was obtained by fitting the results of full valence MRCI+Q/CBS calculations to a modified Morse potential. The interaction potential was described using cutoff "Buckingham" (exp/6) interactions for each pair of intermolecular atoms, with parameters fit to reproduce high-level counterpoise corrected QCISD(T)/CBS interaction energies calculated along six intermolecular CH_4 + O_2 approaches. The fitted exp/6 interaction energies are compared with the QCISD(T)/CBS energies in Fig. 2. In Fig. 2(a), O_2 is oriented radially relative to CH_4 and approaches the face, edge, or vertex of the CH_4 tetrahedron. Similar approaches are shown in Fig. 2(b) where the O_2 is oriented perpendicularly to CH_4. Note that there is less anisotropy for M = O_2 than for M = H_2O, and the simplified separable pairwise exp/6 interaction potential reproduces the high-level energies for M = O_2 fairly accurately.

Trajectory calculations. Ensembles of 500 direct trajectories for M = H_2O and 10,000 trajectories for M = O_2 were prepared at each of four fixed bath gas temperatures T = 300, 1000, 2000, or 3000 K, with initial conditions as described in detail elsewhere.[42] Briefly, for each trajectory CH_4 was assigned an initial rotational state J' from a thermal distribution. The initial total energy of CH_4, E', was chosen to be a function of J' and close to the rotationally adiabatic dissociation threshold. Within these constraints, the initial geometries and momenta were determined microcanonically. For the molecular baths, the initial internal coordinates and vibrational and rotational momenta of the baths were selected randomly and uniformly in time from separate equilibration runs using an Andersen thermostat[62] set to T. The impact parameter b was sampled uniformly from 0–$b_{\max}$, with $b_{\max}$ = 8 Å for M = H_2O at T = 1000–3000 K and $b_{\max}$ = 9 Å for M = H_2O at T = 300 K and for M = O_2 at T = 300–3000 K. This bias[63] in b was corrected for when calculating the low-order moments, as discussed below. The initial and final center-of-mass separations of CH_4 + M were set to 11 Å. At these separations, the bath molecule does not interact appreciably with CH_4, and the final state of CH_4 (E,J) may be calculated unambiguously. The trajectory code (DiNT) and analytic potential energy surfaces used here are available online.[64]

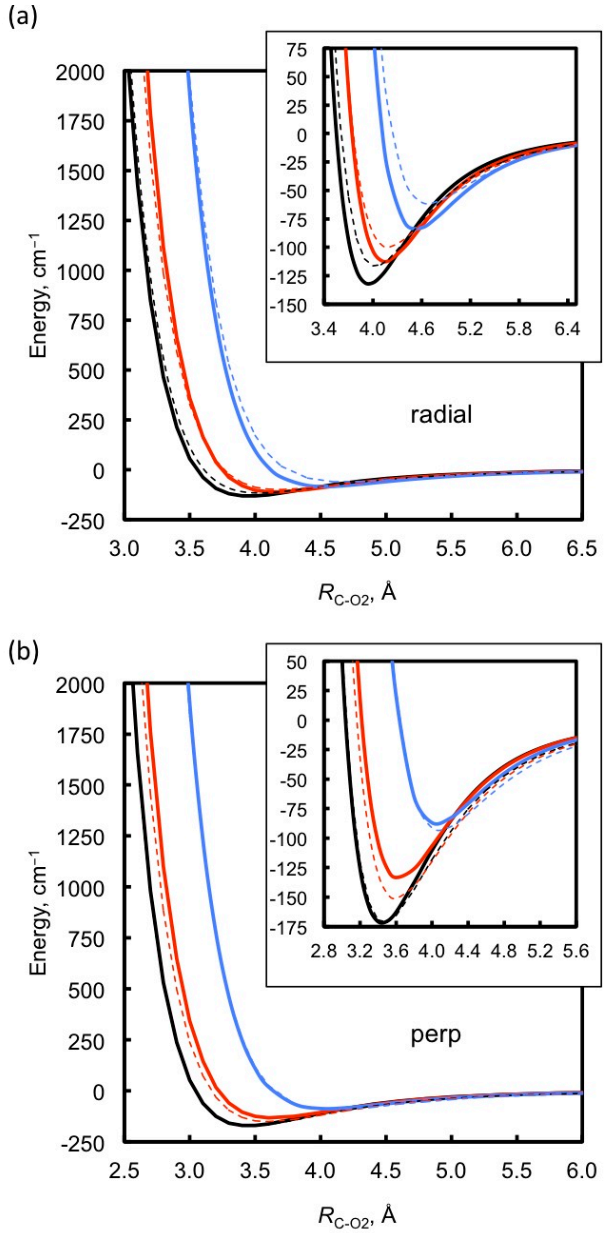

Figure 2. CH_4 + O_2 interaction potential for face (black), edge (red), and vertex (blue) (a) radial and (b) perpendicular approaches. The solid lines are QCISD(T)/CBS energies, and the dashed lines are the fitted exp/6 energies. The insets highlight the van der Waals well.

Per-collision energy and angular momentum transfer moments of order *n* were calculated from the trajectories as

$$< \Delta X^n > = \frac{Z_{\text{HS}}}{Z} \sum_{i=1}^{N} w_i^b \Delta X^n{}_i / N \, , \qquad (1)$$

where Z_{HS} is the hard sphere collision frequency evaluated for the collision diameter b_{max}, Z is the Lennard-Jones collision frequency, $X = E$ or J, $\Delta X = X - X'$, N is the size of the ensemble, i labels trajectories, and the weights $w_i^b = 2b_i / b_{max}$ correct for the artificial sampling of the impact parameter b. One-sigma statistical uncertainties are reported, as estimated using the bootstrap resampling method.[65,66] The per-collision moments in eq 1 are scaled to Lennard-Jones collision rate coefficients, Z, which were calculated from Lennard-Jones parameters obtained using the full-dimensional intermolecular potentials discussed above and the "one-dimensional minimization" method of Ref. 67. This method was shown to predict collision rate coefficients in good agreement with those based on tabulated Lennard-Jones parameters for a wide variety of systems, typically within ~10%. The calculated Lennard-Jones parameters and collision rate coefficients are summarized in Table 1. Also shown are approximate capture rate coefficients, Z_{cap}, calculated using the method of Ref. 68, which was found to be useful for characterizing the kinetics of HO_2 (+M).[69] For the present systems, Z_{cap} = (1.1–1.9) Z, with larger differences at lower temperatures. We will primarily use Z as the chosen collision rate coefficient for scaling the trajectory results, and a brief discussion of the effect of instead using Z_{cap} will be given below.

Table 1. Calculated binary CH_4 + M Lennard–Jones collision parameters (cm^{-1} and Å), collision rate coefficients, and capture rate coefficients (10^{-10} cm^3 $molecule^{-1}$ s^{-1})

M	ε	σ	Z (300 K)	Z_{cap} (300 K)	Z (2000 K)	Z_{cap} (2000 K)
He	21.33	3.328	4.03	6.21	7.70	8.52
Ne	46.75	3.308	2.80	4.78	5.12	6.56
Ar	112.9	3.535	3.49	6.46	5.96	8.81
Kr	138.6	3.644	3.62	6.77	6.06	9.29
H_2	69.48	3.313	6.85	12.2	12.2	16.7
O_2	99.00	3.634	3.69	6.92	6.37	9.49
N_2	99.87	3.670	3.86	6.92	6.66	9.49
CH_4	102.4	3.797	4.68	8.61	8.07	11.8
H_2O	153.9	3.392	4.07	7.66	6.75	10.5

Equation 1 includes all of the trajectories in the ensemble, regardless of outcome. Some models for energy transfer make use of "deactivating" or "activating" moments, where only those trajectories with $\Delta X_i < 0$ or $\Delta X_i > 0$, respectively, are included. These moments will also be presented and are labeled with the subscripts "d" for deactivating (downward) collisions and "u" for activating (upward) collisions.

For sufficiently large $b_{\max}$, the total moments in eq 1 converge with respect to increases in $b_{\max}$. The large-b trajectories necessarily give $\Delta X_i \approx 0$, such that, if $b_{\max}$ is increased, the resulting lowering of the value of the summand in eq 1 is analytically corrected for via a corresponding increase in Z_{HS} ($\propto b_{\max}^2$). Some additional care is required in converging practical calculations of the activating and deactivating moments with respect to $b_{\max}$. For the analytic cancellation discussed above to work correctly for activating and deactivating moments, the "zeros" at large b must be equally distributed as small positive and small negative numbers. Small but systematic integration errors can lead to uneven distributions and seemingly poor convergence of these moments with respect to $b_{\max}$. We emphasize that this issue cannot be conveniently fixed by integrating the trajectories more accurately, as the large-b "zeros" have very small magnitudes at the values of $b_{\max}$ considered here. Instead, we introduce a numerical cutoff parameter, δE, such that when $|\Delta E_i| < \delta E$, ΔE_i is reassigned evenly to either $+\delta E/2$ or $-\delta E/2$. A similar cutoff parameter, δJ, is used to reassign small values of $|\Delta J_i|$. Good convergence of the activating and deactivating moments with respect to $b_{\max}$ was observed with these cutoffs in place, so long as δX was set larger than typical integration errors. Several values of δE and δJ were tested, and the resulting moments were not sensitive to this choice, as δX is much smaller than the calculated moments. For the results reported in Sec. III, $\delta E = 2\ \mathrm{cm}^{-1}$ and $\delta J = 0.02\ \hbar$.

The per-collision moments in eq 1 are referenced to Lennard-Jones collision rates, as discussed above. Although it is conventional to present collisional information this way, it is also convenient to consider average collisional transfer rates, which are defined as

$$r_{\Delta X^n} \equiv Z < \Delta X^n > . \tag{2}$$

Note that Z appears in eqs 1 and 2 in such a way that it cancels out when evaluating $r_{\Delta X^n}$ using trajectories—the calculated values of $r_{\Delta X^n}$ are in fact *independent* of the chosen collision rate Z, whereas the per-collision moments in eq 1 are not.

The state-to-state collisional rate coefficient, $k_c(E,J;E',J')$. Within the usual statistical assumptions about microcanonical ensembles, pressure-dependent rate coefficients are most fundamentally characterized via the master equation,[70,71,72] which describes the competition between intramolecular dynamics (reaction, isomerization, etc.) and collisional activation and deactivation. The collisional term appearing in the ME includes collisional state-to-state rate coefficients, $k_{c,m}(E,J;E',J')$, that describe the rate at which bath gas collisions knock the mth chemical species from some internal state (E',J') to some other state (E,J), where E and J are the total energy and total angular momentum, respectively. The reaction considered here contains a single unimolecular species, CH_4, and so the species index m is suppressed below.

By convention, k_c is generally written as the product of a total collision rate coefficient, Z, and a normalized state-to-state collisional transition probability, $P(E,J;E',J')$, where

$$Z \equiv \sum_J \int dE\, k_c(E,J;E',J')\,, \tag{3}$$

Z is assumed independent of the initial state, and

$$k_c(E,J;E',J') = Z\, P(E,J;E',J')\,. \tag{4}$$

Instead of attempting a detailed characterization of k_c or P, we restrict attention to low-order moments of ΔE and ΔJ, which are related to P by[26]

$$< \Delta X^n >= \sum_{J,J'} \int dE\, \Delta X^n g'(J') P(E,J;E',J') \tag{5}$$

where $g'(J')$ is the initial rotational distribution and is taken here to be a thermal one. The moments in eq 5 are not averaged over the initial energy, E', and instead E' is set to an energy near the rotational threshold; this is equivalent to neglecting the dependence of eq 5 on E'. The present strategy avoids difficulties in dealing with the elastic spike (corresponding to ΔE, $\Delta J = 0$) in trajectory reconstructions of binned representations of P.[25,31,51] While it is true that Z can be made arbitrarily large by increasing the elastic spike, the moments defined in eq 5 depend on Z in a trivial way so long as Z is not too small for similar reasons as discussed above for eq 1.

One can reconstruct useful representations of P from the calculated low-order moments of ΔJ and ΔE (or of k_c from $r_{\Delta E^n}$ and $r_{\Delta J^n}$) by comparing eqs 1 and 5,[73] and several detailed models will be considered in other work.[56] The principal focus here is to quantify the collision efficiency of water relative to the other baths using the calculated low-order collision moments. We limit the present study to three simple models for P, as discussed next.

The 1D model for P employs an exponential functional form and the "down" detailed-balance and normalization convention,[32,34] where

$$P \propto \exp(-|\Delta E|/\alpha) \tag{6}$$

for deactivating collisions, the activating wing of P is determined via detailed balance, α is set to the calculated trajectory value of $<\Delta E_d>$, and J-dependence is not explicitly included. Our implementation of this model (the "E" model of Ref. 44) is strictly one-dimensional as far as the master equation is concerned. It includes J-dependence in the threshold energies, but collisions involving changes in J are completely ignored. The one-dimensional (E-resolved) master equation is solved to obtain phenomenological rate coefficients, as discussed elsewhere.[2]

The 2D/φ model for P also employs an exponential functional form for ΔE and includes J-dependence using a microcanonical statistical model for the post-collision J distribution, φ, i.e.,

$$P \propto \exp(-|\Delta E|/\alpha)\varphi\,, \tag{7}$$

again for deactivating collisions, with detailed balance and normalization enforced and $\alpha = <\Delta E_d>$. The 2D/φ model[43,44] is a "microcanonical strong-collider-in-J" model, where the outcome of the collision is assumed to be statistical and independent of the initial rotational state J'. The model should be distinguished from the "canonical strong-collider-in-J" model discussed in Ref. 42, which was called the ε,J model there and might also be referred to as the 2D/Φ model. The assumption in φ (or Φ) that P is independent of the initial rotational state reduces the two-dimensional (E,J-resolved) master equation to an effective one-dimensional one, which can be solved by the same methods as the 1D master equation.[2]

Finally, we consider a simple example of an explicitly two-dimensional (2D) master equation model, where

$$P \propto \exp(-|\Delta E|/\tilde{\alpha})\exp(-|\Delta J|/\tilde{\gamma})\,, \tag{8}$$

and $\tilde{\alpha}$ and $\tilde{\gamma}$ are determined from $<\Delta E_d>$ and $<\Delta J_d>$. Similar two-dimensional forms have been used previously.[34,58,59] Here we have used the strategy of Ref. 58 for enforcing detailed balance in the two-dimensional master equation along with the "symmetrized" convention for detailed balance[31] (as opposed to the "down" convention used in the 1D and 2D/φ models). The low-pressure-limit 2D master equation using eq 8 for P was solved by iteration of the steady-state populations. When detailed balance and normalization are included, the 2D model in eq 8 is equivalent to the 2D/φ model in eq 7 (not eq 6) in the limit of large γ. Because the symmetrized convention for detailed balance is used in eq 8 and due to the lower bound on J of 0, the range parameters in eq 8 are not equal to the values of the calculated deactivating moments. Instead, $\tilde{\alpha}$ and $\tilde{\gamma}$ were fit such that eq 5 with eq 8 reproduced the calculated trajectory values of $<\Delta E_d>$ and $<\Delta J_d>$. More detailed 2D models for P will be considered in a separate publication.[56]

The term "relative collision efficiency" can mean different things in different contexts.[33] This is in part because so little previous theoretical work has attempted quantitative *predictions* of collisional energy transfer and the competing but related definitions are qualitatively similar. In the context of building detailed chemical kinetic models (e.g., of combustion or atmospheric chemistry), the relative collision efficiency is often expressed as a ratio of low-pressure-limit rate coefficients,

$$k_0(\mathrm{M}) / k_0(\mathrm{Ar}), \qquad (9)$$

where Ar has been used as the reference bath in eq 9. The relative efficiencies in eq 9 will in general depend on the model for P used to calculate k_0; we evaluate eq 9 using the 1D, 2D/φ, and 2D models discussed above.

Calculating eq 9 requires solving the master equation, and it is of interest to consider approximate relative collision efficiencies that are simpler to evaluate. The 1D and 2D/φ master equation models require only the single collisional parameter α, which is set to the average energy transferred in deactivating collisions, $<\Delta E_d>$. One might therefore also consider relative efficiencies approximated as

$$<\Delta E_d>(\mathrm{M}) / <\Delta E_d>(\mathrm{Ar}), \qquad (10)$$

where, again, Ar has been used as the reference bath.

For sufficiently weak collisions and when angular momentum changes are neglected, one can show that the low-pressure-limit rate coefficient depends sensitively only on the low-order moments of ΔE.[32,37] For numerical reasons and because ΔE is typically close to zero, ΔE^2 is more convenient to work with than ΔE in the present context.[26] Consequently, we also consider approximate relative efficiencies given by

$$<\Delta E^2>(\mathrm{M}) / <\Delta E^2>(\mathrm{Ar}). \qquad (11)$$

As discussed above, the definition of Lennard-Jones collision rates is conventional but somewhat arbitrary. It may be more kinetically relevant to consider the per-time energy transfer moments than the per-collision moments in eqs 9 and 10 and so we also consider relative efficiencies given by

$$r_{\Delta E_d}(\mathrm{M}) / r_{\Delta E_d}(\mathrm{Ar}) = Z(\mathrm{M}) < \Delta E_d > (\mathrm{M}) / Z(\mathrm{Ar}) < \Delta E_d > (\mathrm{Ar}) \qquad (12)$$

$$r_{\Delta E^2}(\mathrm{M}) / r_{\Delta E^2}(\mathrm{Ar}) = Z(\mathrm{M}) < \Delta E^2 > (\mathrm{M}) / Z(\mathrm{Ar}) < \Delta E^2 > (\mathrm{Ar}). \qquad (13)$$

The relationship between k_0 and low-order moments of the energy transfer function has been analyzed in detail by Troe.[34,35] Troe found solutions to the master equation as corrections to the strong-collider (SC) (in-E) rate coefficient. In the strong collider limit, eq 9 reduces to the ratio of collision rates

$$Z(\mathrm{M}) / Z(\mathrm{Ar}). \qquad (14)$$

Useful expressions for "weak collider" corrections to the SC rate coefficient have been given as functions of low-order moments of ΔE.[32,33,34] For very weak collisions (i.e., in the weak collision or diffusion limit[37,74]) and employing the single exponential down model with the range parameter $\alpha = <\Delta E_\mathrm{d}>$, the relative collision efficiencies are given by eq 12. For stronger but still weak collisions, the effect of saturation of collision outcomes above threshold must be included,[32,33,34] such as in the following expression given by Troe as a correction to the strong collider rate coefficient[34,35]

$$\beta_c = \left(\frac{\alpha}{\alpha + F_E k_B T} \right)^2 , \qquad (15)$$

where F_E is related to the thermal fraction of unimolecular states above the reaction threshold. Using eq 15, the relative efficiencies in eq 9 are given by

$$Z\,\beta_c(\mathrm{M}) / Z\,\beta_c(\mathrm{Ar}). \qquad (16)$$

Equation 15 was obtained by considering solutions to the 1D master equation. Troe provided analogous expressions for solutions to a version of the 2D master equation, but these are not considered here.

The relative efficiencies defined by eq 9 and the approximations to eq 9 given by eqs 10–13 are presented next in Sec. III. Newly reported results for M = H_2O and O_2 are compared with previously reported results[42] for M = He, Ne, Ar, Kr, H_2, N_2, and CH_4. New ensembles of trajectories were calculated for several of the previously considered baths, and more detailed collisional transfer moments are reported here than previously. The bath M = CO was previously considered, but detailed new results for M = CO are not included here due to significant uncertainties in its potential energy surface parameterizations, as discussed previously.[42]

III. Results and Discussion

Calculated first and second moments of ΔE are shown in Table 2 for M = H_2O and O_2. The relatively small ensemble size for the direct dynamics trajectories for M = H_2O is sufficient to converge the moments to ~10%. Similar tables summarizing the results of trajectory calculations for the previously studied baths are included as supporting information; the new trajectory results agree with those reported in Ref. 42 subject to their statistical uncertainties and small differences in the choice of Z in the two studies. Trends in the magnitude and temperature dependence of the energy transfer moments for CH_4 + M calculated using the trajectory methods described in Sec. II have been discussed in detail previously,[42] and such a discussion is not reproduced here. Instead, we note that the present results for the newly considered baths generally agree with the previously reported trends. Briefly, the calculated energy transfer moments for M = O_2 are very similar to those for M = CO and N_2. The energy transfer moments for the polyatomic collider M = H_2O are larger than those for the atomic and diatomic baths and are close to, but typically larger than, those previously reported for another polyatomic collider M = CH_4.

Table 2. Low-order collisional energy transfer moments (cm^{-1}) for M = H_2O and O_2

M	T, K	$-\langle\Delta E_d\rangle$	$\langle\Delta E_u\rangle$	$\langle\Delta E^2\rangle^{1/2}$	$\langle\Delta E_d^2\rangle^{1/2}$	$\langle\Delta E_u^2\rangle^{1/2}$
H_2O	300	737 ± 85	289 ± 33	541 ± 53	686 ± 74	269 ± 37
	1000	1265 ± 125	683 ± 66	813 ± 57	990 ± 92	607 ± 48
	2000	1846 ± 209	1189 ± 106	1348 ± 146	1637 ± 231	961 ± 77
	3000	2333 ± 176	1598 ± 107	1840 ± 119	2185 ± 187	1370 ± 97
O_2	300	167 ± 2	129 ± 2	167 ± 2	181 ± 3	151 ± 2
	1000	329 ± 6	313 ± 5	391 ± 5	401 ± 8	382 ± 7
	2000	573 ± 11	541 ± 10	695 ± 9	710 ± 14	680 ± 13
	3000	809 ± 15	775 ± 14	988 ± 14	1010 ± 20	966 ± 20

The 1D and 2D/φ models require the single parameter $\alpha = \langle \Delta E_d \rangle$, which is often written as the two-parameter expression

$$\alpha(T) = \alpha_{300}(T/300\,\mathrm{K})^{n_\alpha}. \qquad (17)$$

The trajectory-based moments in Table 2 are reasonably well represented by eq 17 with α_{300} = 720 cm^{-1} and n_α = 0.5 for M = H_2O and α_{300} = 140 cm^{-1} and n_α = 0.76 for M = O_2. This temperature dependence for M = O_2 is consistent with that of M = N_2 and CO (also fit with n_α = 0.76 in Ref. 42) and is similar to that of the heavier atomic baths (results for Ar and Kr were fit with n_α = 0.75 and 0.67, respectively). The lighter baths show a stronger temperature dependence, with n_α = 0.95 for M = He and n_α = 0.83 for M = H_2. The weakest temperature dependence is found for the polyatomic baths, with M = H_2O featuring somewhat less temperature dependence than M = CH_4 (n_α = 0.6).

Table 3. Low-order collisional angular momentum transfer moments ($\hbar$) for M = H_2O and O_2

M	T, K	$-\langle \Delta J_d \rangle$	$\langle \Delta J_u \rangle$	$\langle \Delta J^2 \rangle^{1/2}$	$\langle \Delta J_d^2 \rangle^{1/2}$	$\langle \Delta J_u^2 \rangle^{1/2}$
H_2O	300	3.36 ± 0.39	4.43 ± 0.33	3.67 ± 0.19	2.68 ± 0.30	4.18 ± 0.25
	1000	5.56 ± 0.64	4.29 ± 0.32	4.22 ± 0.23	4.26 ± 0.41	4.19 ± 0.27
	2000	5.96 ± 0.64	4.89 ± 0.43	5.02 ± 0.32	5.07 ± 0.51	4.98 ± 0.41
	3000	6.88 ± 0.56	5.97 ± 0.38	6.12 ± 0.32	6.18 ± 0.44	6.07 ± 0.44
O_2	300	2.28 ± 0.04	3.14 ± 0.04	2.96 ± 0.03	2.44 ± 0.04	3.33 ± 0.04
	1000	2.99 ± 0.05	3.28 ± 0.05	3.58 ± 0.04	3.40 ± 0.06	3.74 ± 0.06
	2000	3.72 ± 0.07	4.00 ± 0.07	4.48 ± 0.05	4.30 ± 0.07	4.65 ± 0.08
	3000	4.42 ± 0.08	4.54 ± 0.08	5.19 ± 0.07	5.16 ± 0.10	5.22 ± 0.08

Low-order moments of ΔJ were not previously reported in Ref. 42. Other workers have calculated similar quantities using classical trajectories,[25,31,53,54] and the role of angular momentum in unimolecular reactions has been discussed in detail.[31,34,3243,44] Here we quantify some of the effects of angular momentum on unimolecular reactions using the collision models discussed above along with calculated angular momentum transfer moments. Table 3 presents first and second moments of ΔJ for M = H_2O and O_2, with results for the other baths again included as supporting information. The magnitudes of the low-order moments of ΔJ vary from 2–8 $\hbar$ and increase with temperature. Notably, the low-order moments of ΔJ vary less with the choice of bath gas than those of ΔE. M = H_2O is generally a stronger collider in J than the other baths. M = He, Ne, and sometimes H_2 feature slightly stronger temperature dependence than the other baths for the moments of ΔJ. Overall, baths other than M = H_2O are qualitatively similar to one another in their predicted total angular momentum transfer moments.

The 2D collision model discussed above (eq 8) was parameterized to reproduce the calculated values of $<\Delta J_\mathrm{d}>$ and $<\Delta E_\mathrm{d}>$. A two parameter (γ_{300} and n_γ) expression for $\gamma = <\Delta J_\mathrm{d}>$ analogous to the one used for α in eq 17 was adopted here to allow for convenient comparisons of the different baths. Results for M = He show the strongest temperature dependence in γ with the trajectory values reproduced well by $\gamma_{300} = 1.84$ $\hbar$ and $n_\gamma = 0.41$. Results for M = Ne show somewhat weaker temperature dependence, with $\gamma_{300} = 2.05$ $\hbar$ and $n_\gamma = 0.35$. The other baths are reproduced reasonably well with $n_\gamma = 0.30$ and γ_{300} = 2.05, 2.05, 2.00, 2.15, 2.15, 2.15, and 3.60 $\hbar$ for M = Ar, Kr, H_2, N_2, O_2, CH_4, and H_2O, respectively. The most notable result for γ is that M = H_2O is qualitatively a stronger collider in J than the other baths, while the other baths are similar to one another in their collision efficiencies in J. The collision efficiency in J appears to be independent of the strength of the collider in E. For example, M = CH_4 is qualitatively a stronger collider in E than the atomic and diatomic baths, but it is very similar to the atomic and diatomic baths in its collision efficiency in J. Another notable result is that the fitted values of n_γ range from 0.3–0.4, whereas n_α varies from 0.5–1.0. The different temperature dependence of α and γ gives rise to a temperature-dependent weak-collider-in-J effect, as quantified below.

In Fig. 3, the calculated values of $<\Delta J_\mathrm{d}>$ for M = He, O_2, and H_2O are compared with two analytic limits for $<\Delta J_\mathrm{d}>$. One may write a simple analytic expression for $<\Delta J_\mathrm{d}>$

$$<\Delta J_\mathrm{d}> = \int_0^\infty dJ' g'(J') \int_0^{J'} dJ g(J)\, \Delta J\,, \tag{18}$$

where $g'(J')$ is the initial distribution of angular momentum, which, as in the trajectory calculations is taken to be a thermal distribution, and $g(J)$ is the final distribution of angular momentum that results from the collisions. (Note that one might choose to write eq 18 using sums instead of integrals; the meaning of eq 18 would be unchanged.) The first analytic limit we consider is a microcanonical statistical one with

$$g(J) \propto \rho(E_J, J)\,, \tag{19}$$

where $\rho(E_J, J)$ is the rovibrational state density of CH_4 evaluated at the rotationally adiabatic threshold for dissociation E_J. The second analytic limit assumes a thermal distribution of independent rotations for $g(J)$. One expects the maximum possible value of $<\Delta J_d>$ calculated via the trajectory ensembles used here to be related to the thermal limit, whereas the microcanonical statistical limit might be more relevant to the 2D/φ model. As shown in Fig. 3, the microcanonical and thermal limits are similar to one another, and we focus the present discussion on comparisons with the microcanonical statistical limit. At 300 K, the trajectory-based values of $<\Delta J_d>$ are 30–60% of the microcanonical limit for all the baths considered here except for M = H_2O, for which the calculated value of $<\Delta J_d>$ is close to the microcanonical limit. The trajectory-based value of $<\Delta J_d>$ at 1000 K is again very close to the microcanonical limit for M = H_2O and is only half that value for the other baths. At higher temperatures, the calculated values of $<\Delta J_d>$ for M = H_2O deviate from the microcanonical limit but are still twice as large as those of the other baths.

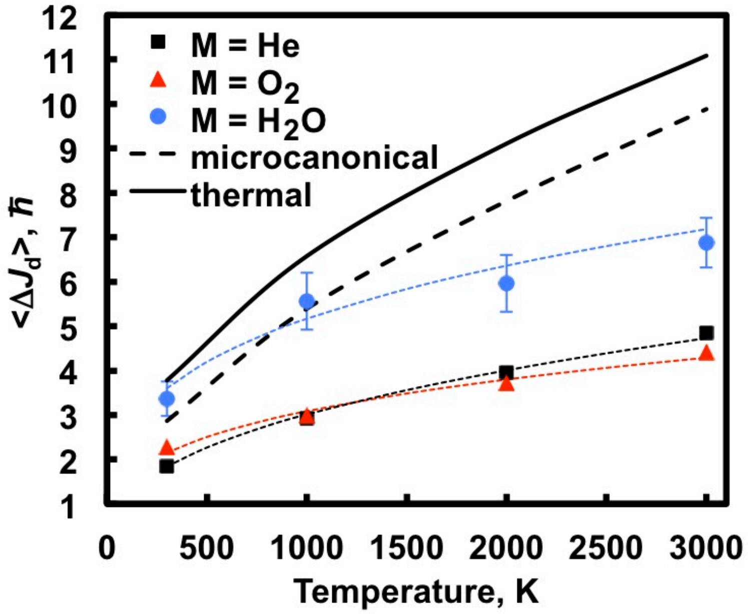

Figure 3. $<\Delta J_d>$ calculated via classical trajectories for three baths (He: black squares; O_2: red triangles; H_2O: blue circles) and the associated two-parameter fits (dotted lines). The thick lines are the microcanonical (dotted) and thermal (solid) limits.

Again, water is qualitatively more efficient than the other baths in equilibrating rotations. Below 1000 K, water is efficient enough to fully equilibrate rotations, whereas above 1000 K microcanonical statistical assumptions (as in the 2D/φ model) for the rotational distribution resulting from M = H_2O collisions may not be supported. Statistical assumptions for the other baths may be similarly questioned, even at low temperatures. We will see next, however, that the *kinetic* effect of these weak collisions "in J" can be small even when the calculated value of $<\Delta J_d>$ is not close to its statistical limit.

Low-pressure-limit rate coefficients were calculated using the three models for P discussed above: the one-dimensional (1D) model; the two-dimensional (2D/φ) model, which employs a microcanocial statistical model for J; and the two-dimensional (2D) model of eq 8, which explicitly includes weak-collider-in-J effects. Here, we limit attention to the baths M = He, O_2, and H_2O when comparing the results of the three models for P. The calculated values of k_0 using the 1D and 2D/φ models are shown in Fig. 4 relative to k_0 for the 2D model as functions of temperature. The 1D model overpredicts the 2D value of k_0 for all three baths by as much as a factor of 6 at low temperatures. The magnitude of this effect is similar to but somewhat larger than differences in the 1D and 2D/φ models reported previously.[44,75,76,77,78,79] The 2D/φ model is a significant improvement over the 1D model and differs substantively from the 2D model only at low temperatures for M = He and O_2. As discussed above, the trajectory-based values of $<\Delta J_d>$ are close to their statistical limits for M = H_2O at low temperatures but not for M = He and O_2. Figure 4 confirms that the results of the 2D/φ and 2D models are in very close agreement with one another for M = H_2O at low T, whereas there are non-negligible differences at low T for M = He and O_2 due to incomplete collisional rotational equilibration. The 2D/φ and 2D values of k_0 are very similar to one another above ~1500 K, however, for all three baths, even though the trajectory values of $<\Delta J_d>$ are not close to their statistical limits at these temperatures. This suggests that the weak collider in J effect is less important at higher temperatures.

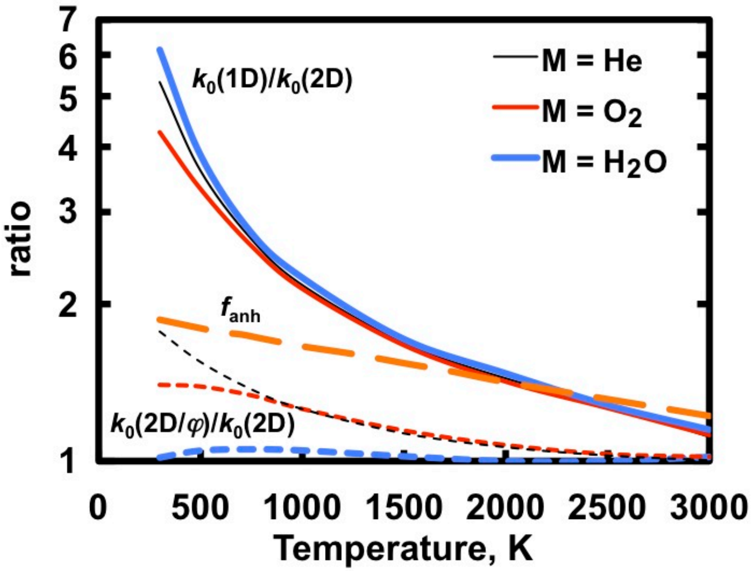

Figure 4. Low-pressure-limit rate coefficients for the 1D model (solid lines) and the 2D/φ model (dotted lines) relative to those for the 2D model for three baths: He (thin black lines), O_2 (red lines), and H_2O (thick blue lines). The vibrational anharmonicity correction (f_{anh}) for CH_4 dissociation (taken from Ref. 6) is shown as a thick orange dashed line.

In summary, while Fig. 3 demonstrates that rotations are not fully equilibrated at elevated temperatures for any of the baths or at low temperatures for any of the baths other than water, Fig. 4 demonstrates that the *kinetic* effect of weak collisions in J is significant only at low temperatures. The 2D/φ model is therefore accurate for many applications, including many combustion applications. At room temperature, however, where theoretical/experimental comparisons are often made, more detailed theoretical models may be required for quantitative predictions.

Low-pressure-limit and pressure-dependent falloff rate coefficients calculated using the 2D/φ model and trajectory-based values of α were previously compared[42] with experimental rate coefficients for M = He, Ar, and CH_4. Agreement was good overall, but we noted that a more accurate treatment of vibrational anharmonicity would have increased the low-pressure-limit rate coefficient by a factor of two, which would have resulted in worse agreement with experiment for M = He at low temperatures but better agreement for M = Ar at elevated temperatures. Figure 4 includes a plot of the temperature dependent rovibrational anharmonicity correction to k_0, f_{anh}, taken from Ref. 6. This correction is equal to the rovibrational anharmonicity correction to the state density of CH_4 at its dissociation threshold divided by the correction to the thermal partition function of CH_4. For M = He at 300 K, the error due to the neglect of vibrational anharmonicity is nearly equal to the error due to the use of the statistical assumption for J, i.e., due to the use of the 2D/φ model. These errors have opposite signs such that the neglect of both of these effects in the calculations of Ref. 42 explains the previous excellent agreement with the experiment. The error due to the weak-collider-in-J effect differs for the three bath gases and falls off more quickly with temperature than the error associated with the neglect of vibrational anharmonicity. One may therefore expect the calculations reported in Ref. 42 to underpredict experiment at elevated temperatures for M = He and for other baths; these qualitative trends were indeed observed. Clearly, the near quantitative cancellation demonstrated here for M = He at 300 K cannot be relied upon in general.

Next, the collision efficiency of water is compared with eight other baths. In Fig. 5, relative values of k_0 at 300 and 2000 K are shown for nine baths with M = Ar chosen as the reference bath. Several models for k_0 were considered. Although there can be significant differences in the values of k_0 calculated using the 1D, 2D/φ, and 2D master equation models (as discussed above and shown in Fig. 4), the *relative* values predicted by the three models are very similar to one another for all the baths except for M = H_2O and CH_4 at 300 K. Differences in the predictions of the 1D and 2D models are generally more significant for larger values of α/k_BT, which explains the larger discrepancy seen here for M = H_2O and CH_4 at low T.

As shown in Fig. 5, Troe's weak collider model (with relative efficiencies given by eq 16) very accurately predicts the 1D master equation results, as it was designed to do. As noted above, Troe also formulated approximations to the 2D master equation,[32] but we have not considered them here. At 300 K, the calculated values of β_c range from 0.15–0.20 for all the baths except M = CH_4 ($\beta_c = 0.37$) and M = H_2O ($\beta_c = 0.60$). At 2000 K, $\beta_c = 0.04$–0.08 for all the baths except M = CH_4 ($\beta_c = 0.13$) and M = H_2O ($\beta_c = 0.27$). We conclude that for sufficiently weak collisions (say, for $\beta_c < 0.2$) the 1D formulation of the master equation and Troe's analytic solution to it may be used to reliably calculate *relative* collision efficiencies. For stronger collisions ($\beta_c > 0.2$), solving a 2D formulation of the master equation may be required for quantitative predictions.

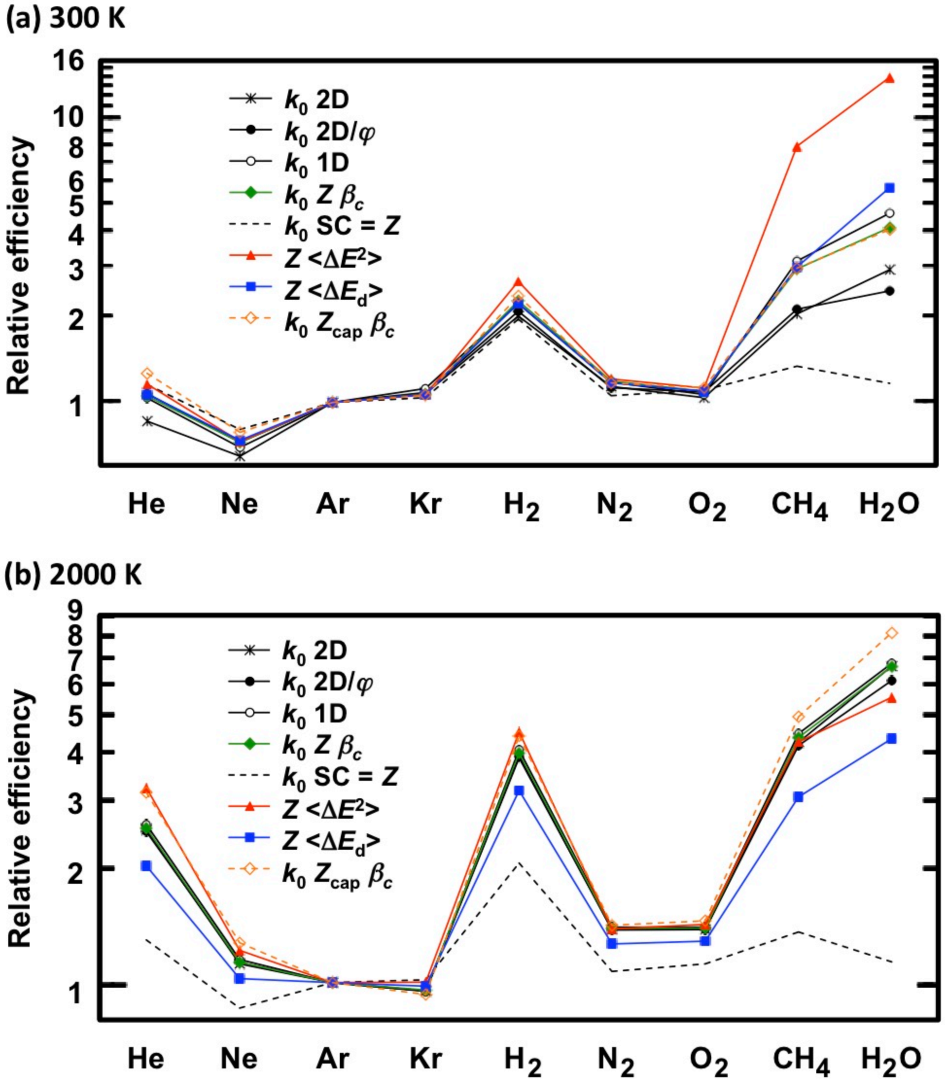

Figure 5. Relative collision efficiencies ($k_0(M)/k_0(Ar)$) for three master equation models (1D, 2D/φ, and 2D), for the strong collider model (SC), and for the weak collider model of Troe ($Z\,\beta_c$) at (a) 300 K and (b) 2000 K. Also shown are the results of the weak collider model calculated using Z_{cap} and the relative low-order moments <ΔE^2> and <ΔE_d>. The low-order moments have been scaled by Z for a more meaningful comparison with k_0.

Relative values of the strong collider (SC) rate coefficient are equal to the relative values of the collision rates (Z) (eq 14) and are not useful in predicting relative collision efficiencies, as shown in Fig. 5. This information can be useful, however, for identifying the relative importance of two different sources of enhanced collision efficiency. Enhanced collision efficiency may be attributed to enhanced energy transferred per collision, more collisions per time, or both. At 300 K, for example, M = H_2 is twice as efficient as M = Ar, which is correctly predicted by the relative magnitudes of Z for these two baths. M = H_2O is also twice as efficient as M = Ar at 300 K, but $Z(H_2O)/Z(Ar)$ is close to unity. We may attribute the enhanced efficiency for M = H_2

relative to M = Ar to an increase in the collision frequency due to its lighter mass, whereas the enhanced efficiency for M = H_2O relative to M = Ar is attributed to an increase in the energy transferred per collision. We note that inherent ambiguities in the definition of a collision complicate quantifying the relative importance of these two effects.

As discussed in Sec. II, it may be preferable to use a capture rate coefficient (such as the approximate capture rate coefficients, Z_{cap}, of Refs. 68 and 69) to scale the trajectory results instead of the Lennard-Jones collision rates, Z. The results of Troe's weak collider model using Z_{cap} are shown in Fig. 5. To obtain these results, β_{c} was recalculated using values of $<\Delta E_{\mathrm{d}}>$ obtained via an equation analogous to eq 1 but with Z_{cap} in place of Z. As seen in Fig. 5, relative collision efficiencies obtained using Z_{cap} are very similar to and occasionally slightly larger than the results obtained using the Lennard-Jones collision rate coefficient, Z. We may conclude that relative collision efficiencies are fairly insensitive to the choice of the collision rate coefficient used to scale the trajectory results.

The per-collision energy transfer moments in eqs 10 and 11 are poor predictors of $k_0(\mathrm{M})/k_0(\mathrm{Ar})$ due to the neglect of the effect of Z on k_0 for the reasons given just above. The results of eqs 10 and 11 are therefore not plotted in Fig. 5. Because eq 10 is sometimes used to approximate relative efficiencies, we note that including the effect of Z when calculating relative collision efficiencies (as in eq 12) systematically improves the accuracy of the estimated relative values of k_0 as compared with eq 10.

The results of eqs 12 and 13 are shown in Fig. 5. These methods can be qualitatively useful in predicting the results of the more complete calculations, but neither scaled moment is predictive. In fact, the relative values of $Z <\Delta E^2>$ are significantly in error for the stronger colliders at 300 K, predicting an enhancement of 14 instead of 3 for M = H_2O relative to M = Ar. In contrast, the value of $Z <\Delta E_{\mathrm{d}}>$ for M = H_2O relative to M = Ar is 50% too small at 2000 K. Again, Troe's formulation, which involves a simple function of $<\Delta E_{\mathrm{d}}>$ (eq 15) and requires only slightly more effort than eq 12 to evaluate due to F_E, is systematically more accurate than either eq 12 or 13.

M = H_2O is the strongest collider considered here, with low-pressure-limit rate coefficients that are 3–7x larger than those for M = Ar. The relative efficiency varies as a function of temperature and, perhaps surprisingly, larger differences are found at higher temperatures. The trend with temperature is *not* predicted correctly by the trends in the scaled low-order energy transfer moments, as shown in Fig. 5. This discrepancy (and the poor performance of the low-order moments in predicting relative collision efficiencies in general) may be explained by noting that, for strong enough colliders, the number of states above threshold limits the dissociation rate, at least partially. This effect is included in the expression given by Troe for β_c (eq 15), where it can be seen that for weak colliders ($\alpha << F_E k_B T$) β_c (and therefore k_0) is proportional to α^2, whereas for stronger colliders ($\alpha > F_E k_B T$) β_c varies with α less than quadratically. For the present systems, $F_E k_B T$ = 220 and 1900 cm^{-1} at 300 and 2000 K, respectively (taken from Ref. 7). The present values for α and $F_E k_B T$ cause β_c to vary approximately linearly with α for the weaker colliders and less than linearly with α for the stronger colliders. Properly accounting for the saturation of collision outcomes requires either solving the master equation or using an approximate analytic solution to one, such as Troe's β_c.

As noted in the Introduction, the collision efficiency of water has been found to be as much as 20x as large as typical atomic and diatomic baths for some systems, such as H_2O (+ H_2O)[46] and HO_2 (+ H_2O).[47] This "water enhancement effect" is much larger than the enhancement reported here of only 3–7x. Systems such as H_2O and HO_2 have stronger interactions with water (arising from dipole-dipole interactions, hydrogen bonding, etc…) than those for CH_4 + H_2O (which features a much weaker dipole-induced-dipole interaction). The relative collision efficiencies reported here for H_2O may then be lower bounds on what may be expected generally for polar systems.

Next, a brief mechanistic discussion of the CH_4 + H_2O trajectories is presented, and comparisons are made with CH_4 + He and CH_4 + O_2 trajectories. We first quantify the impact parameter dependence of the cross section for collisional energy transfer by binning and averaging the calculated values of ΔE for deactivating collisions as a function of b. The resulting binned values of $<\Delta E_d(b)>$ are shown in Fig. 6 for the three baths at two temperatures. The binned averages in Fig. 6 are normalized such that the total energy transfer averages in Table 2 are related via

$$< \Delta E_d > \approx \frac{Z_{\mathrm{HS}}}{Z_{\mathrm{LJ}}} \sum_k w_k^b < \Delta E_d(b_k) > / N_k \,, \qquad (20)$$

where k labels the N_k (= 8) bins, the bin width is 1 Å, and $w_k^b = 2b_k / 8\text{Å}$ corrects for the artificially uniform sampling of b.

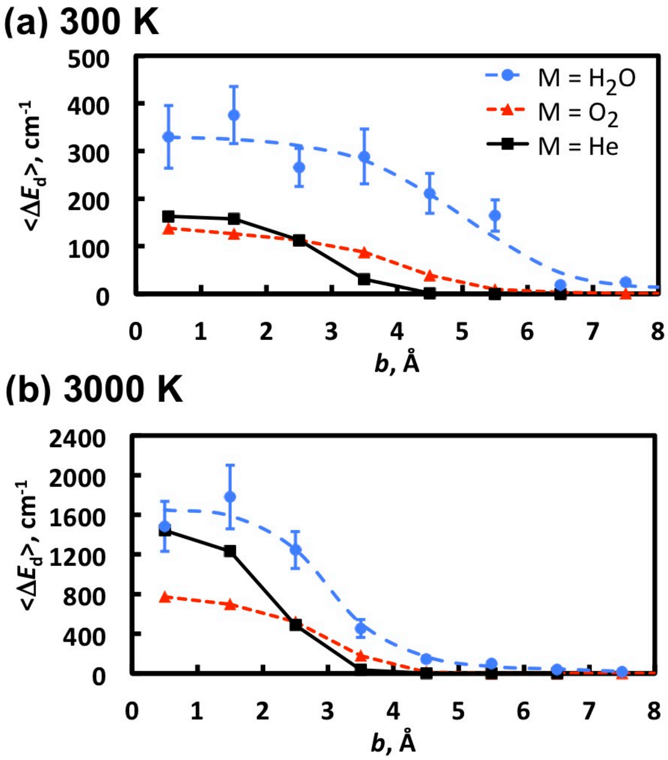

Figure 6. Binned average energy transferred in deactivating collisions as a function of impact parameter at (a) 300 K and (b) 3000 K for three baths: He (black squares), O_2 (red triangles), and H_2O (blue circles). The bin width is 1 Å. Due to the statistical uncertainty in the results for M = H_2O, the thick dashed line was fit to the binned results.

At 300 K (Fig. 6(a)), M = H_2O collisions with appreciable energy transfer are much longer-ranged than those for the other baths, occurring with impact parameters as large as ~6 Å. In addition to this larger collisional energy transfer cross section, M = H_2O collisions also feature stronger "head on" (small *b*) collisions than the other baths. For M = He and M = O_2 small-*b* collisions transfer ~150 cm^{-1} on average in deactivating collisions, while for M = H_2O small-*b* collisions are more than twice as strong. Together, these two effects account for the ~5x larger value of $<\Delta E_d>$ calculated for M = H_2O than for M = He and O_2. We note that M = He and O_2, which have similar overall collision efficiencies at 300 K, have somewhat different collisional energy transfer cross sections. The small-*b* collisions for M = He are somewhat stronger than those for M = O_2, while the collisional energy transfer cross section for M = He is shorter ranged than that for M = O_2. These effects largely cancel, and this is one example of how highly-averaged properties (such as thermal rate coefficients, k_0) do not necessarily depend in simple ways on the various details of the collisions.

At 3000 K (Fig. 6(b)), M = H_2O is again the strongest collider at small *b* as well as the collider with the longest-ranged collisional energy transfer cross section. M = H_2O is 2x as strong of a collider as M = O_2 for small *b*, but, unlike the results at 300 K, small-*b* collisions for M = He are closer to those of M = H_2O than M = O_2. Again, the shorter-ranged collisional energy transfer cross section for M = He results in similar *total* moments for M = He and O_2.

As shown in Fig. 6, in addition to featuring a longer-ranged collisional energy transfer cross section, M = H_2O also features stronger individual collisions. One might associate these stronger collisions with the deeper van der Waals wells on the interaction potential for M = H_2O relative to the other baths (see Figs. 1 and 2 and those in Ref. 42). Strong enough interactions may in fact temporarily "capture" the bath gas and lead to multiple collisions. To quantify this effect, we counted the number of inner turning points of the center-of-mass separation of CH_4–M along each trajectory (i.e., we counted the number of "bounces" per collision) for M = H_2O, O_2, and He at two temperatures.

At 300 K, fewer than 5% of M = H_2O collisions bounced more than once. Neglecting these collisions reduced the calculated value of $<\Delta E_d>$ by only 14%, which is close to the statistical uncertainty of $<\Delta E_d>$. Only 1.5% of M = H_2O collisions were strong enough to remove more than 1000 cm^{-1} from CH_4, and half of these were "direct" collisions, bouncing only once. The two strongest deactivating M = H_2O collisions (i.e., those with the two largest negative values of ΔE) did show multiple collisions. These trajectories were the only ones to remove more than 1500 cm^{-1} from CH_4 and bounced 11 ($\Delta E = -2474$ cm^{-1}) and 14 ($\Delta E = -1831$ cm^{-1}) times. The importance of so-called supercollisions (i.e., rare but strong collisions comprising the "long tail" of *P*) and their relationship to these "chattering" collisions have been discussed previously.[25,54,80,81,82]

As may be expected due to their weaker interaction potentials, similar analyses for M = He and O_2 at 300 K find far fewer indirect trajectories than for M = H_2O, with only 0.2% of M = He trajectories and 0.5% of M = O_2 trajectories bouncing more than once. The few trajectories that did bounce more than once for M = He and O_2 did so only 2–4 times, which is not necessarily indicative of the chattering mechanism.

At 1000 K and above, multiple collision trajectories were not identified for any of the baths, including M = H_2O. We conclude that while one can identify multiple collision trajectories at low temperature for M = H_2O but not for the other baths, this mechanism occurs too infrequently to explain the enhanced energy transfer for M = H_2O.

Some workers have developed statistical models for collisional energy transfer (see, e.g., Ref. 83 and the discussion therein). For the systems considered here, the above analysis indicates that direct collisions dominate the overall energy transfer dynamics and that statistical models of energy transfer may not be accurate. Statistical models may be more appropriate for larger systems, systems with stronger interactions, and collisions at lower temperatures.

V. Conclusions

Trajectory calculations of CH_4 + M collisions were carried out for ensembles relevant to the unimolecular dissociation of CH_4. The low-pressure-limit rate coefficient was characterized via calculated trajectory-based low-order moments of the total energy, E, and angular momentum, J, transferred due to collisions. Direct trajectory results for M = H_2O were compared with results for M = O_2 and with previous results for several baths, M = He, Ne, Ar, Kr, H_2, N_2, and CH_4. Trends in the calculated energy transfer moments were found to be consistent with those reported in past work: the energy transfer moments for the polyatomic collider M = H_2O were larger in magnitude and showed relatively less temperature dependence than those for the atomic and diatomic baths.

Moments of the angular momentum transferred due to collisions were discussed in detail. Specifically, we found that stronger collisions in E do not necessarily result in stronger collisions in J. M = H_2O was shown to be a much stronger collider in J than any of the other baths. In fact, M = H_2O collisions fully rotationally equilibrate J below 1000 K, whereas the other baths do not. Above 1000 K, J was shown to be not fully equilibrated via collisions for any of the baths.

The kinetic effect of these "weak-collider-in-J" collisions was quantified. Specifically, the calculated trajectory moments were used to parameterize three different models of the energy transfer function: a 1D model where angular momentum changes due to collisions are neglected, a 2D/φ model where collisions are assumed to fully equilibrate rotations at fixed energy, and an explicitly 2D model that includes weak-collider-in-J effects. In agreement with previous work, the use of the 1D model was found to lead to significant errors in k_0, shown here to be as large as a factor of 6 at low temperatures. The microcanonical-equilibrium assumption for the rotations (i.e., the 2D/φ model) was found to be very accurate, even when the calculated angular momentum transfer moments are not close to their statistical limits and particularly at elevated temperatures. At room temperature, however—where experimental information is often available—the use of the explicitly 2D master equation model resulted in smaller rate coefficients by 50% relative to the 2D/φ model. This error is on the order of other significant errors in typical kinetics calculations, such as the neglect of vibrational anharmonicity.

The relative collision efficiency for M = H_2O was shown to depend on temperature and to vary from 3–7 from 300–3000 K, where M = Ar was chosen as the reference bath. The magnitude of the present collision efficiency enhancement for water in promoting methane dissociation is smaller than what has been reported elsewhere for other reactions (e.g., H_2O (+H_2O) and HO_2 (+H_2O)), where values as large as 20 have been reported. Because methane is nonpolar and roughly spherical, the present relative collision efficiencies for water may be lower bounds on its general relative collision efficiency. The stronger interactions of H_2O with polar systems and the presence of hydrogen bonding may enhance energy transfer.

Practical detailed chemical kinetic models can require collisional efficiencies for a large number of pressure-dependent reactions. We therefore tested the accuracy of methods for predicting collision efficiencies from the trajectory-based low-order moments that do not require solving the master equation. Troe's weak collider efficiency, β_c, which includes the effect of the number of states above threshold, very accurately predicted the relative collision efficiencies of the eight baths. Simpler functions of the low-order moments were found to be qualitatively useful, but were not generally predictive, particularly for the stronger colliders ($\beta_c > 0.2$).

A discussion of mechanistic details related to energy transfer inferred from the trajectories was given for M = H_2O, O_2, and He. M = H_2O was shown to have both a longer-ranged collisional energy transfer cross section and stronger "head on" collisions. The trajectories were further analyzed by quantifying the importance of the "multiple collision" or "chattering" mechanism relative to direct single collision energy transfer. Trajectories associated with the former mechanism were identified for M = H_2O at 300 K, but their frequency was too low to explain the enhanced energy transfer per collision for M = H_2O. No multiple collision trajectories were found above 300 K for M = H_2O and at any temperature for the other baths.

Supporting Information

Collision rate coefficients, low-order collisional energy transfer moments, and low-order collisional angular momentum transfer moments for CH_4 + M, M = He, Ne, Ar, Kr, H_2, O_2, N_2, CH_4, and H_2O. This information is available free of charge via the Internet at http://pubs.acs.org.

Acknowledgments

We thank Prof. Jürgen Troe for encouraging these calculations. This work is supported by the Division of Chemical Sciences, Geosciences, and Biosciences, Office of Basic Energy Sciences, U.S. Department of Energy. Sandia is a multiprogram laboratory operated by Sandia Corporation, a Lockheed Martin Company, for the United States Department of Energy under Contract No. DE-AC04-94-AL85000. The work at Argonne was supported under Contract No. DE-AC02-06CH11357 as part of the Argonne-Sandia Consortium on High-Pressure Combustion Chemistry (FWP # 59044). Software development was supported by the AITSTME project as part of the Predictive Theory and Modeling component of the Materials Genome Initiative.

Figure Captions

Fig. 1 CH_4 + H_2O interaction potential for face (black), edge (red), and vertex (blue) (a) “O-in” and (b) “H-in” approaches. The solid lines in all four panels are QCISD(T)/CBS energies, and the dashed lines are SAC/aug-cc-pVDZ energies. The insets highlight the van der Waals well.

Fig. 2 CH_4 + O_2 interaction potential for face (black), edge (red), and vertex (blue) (a) radial and (b) perpendicular approaches. The solid lines are QCISD(T)/CBS energies, and the dashed lines are the fitted exp/6 energies. The insets highlight the van der Waals well.

Fig. 3. $<\Delta J_d>$ calculated via classical trajectories for three baths (He: black squares; O_2: red triangles; H_2O: blue circles) and the associated two-parameter fits (dotted lines). The thick lines are the microcanonical (dotted) and thermal (solid) limits.

Fig. 4. Low-pressure-limit rate coefficients for the 1D model (solid lines) and the 2D/φ model (dotted lines) relative to those for the 2D model for three baths: He (thin black lines), O_2 (red lines), and H_2O (thick blue lines). The vibrational anharmonicity correction (f_{anh}) for CH_4 dissociation (taken from Ref. 6) is shown as a thick orange dashed line.

Fig. 5. Relative collision efficiencies (k_0(M)/k_0(Ar)) for three master equation models (1D, 2D/φ, and 2D), for the strong collider model (SC), and for the weak collider model of Troe ($Z\beta_c$) at (a) 300 K and (b) 2000 K. Also shown are the results of the weak collider model calculated using Z_{cap} and the relative low-order moments $<\Delta E^2>$ and $<\Delta E_d>$. The low-order moments have been scaled by Z for a more meaningful comparison with k_0.

Fig. 6. Binned average energy transferred in deactivating collisions as a function of impact parameter at (a) 300 K and (b) 3000 K for three baths: He (black squares), O_2 (red triangles), and H_2O (blue circles). The bin width is 1 Å. Due to the statistical uncertainty in the results for M = H_2O, the thick dashed line was fit to the binned results.

References

[1] Miller, J. A.; Pilling, M. J.; Troe, J. Unraveling Combustion Mechanisms Through a Quantitative Understanding of Elementary Reactions. Proc. Combust. Inst. 2005, *30*, 43–88.

[2] Miller, J. A.; Klippenstein, S. J. Master Equation Methods in Gas Phase Chemical Kinetics. J. Phys. Chem. A 2006, *11*, 10528–10544.

[3] S. J. Klippenstein, “Advances in Theory of Combustion,” US National Combustion Meeting, Atlanta, GA, March 23, (2011).

[4] Pilling, M. J. Reactions of Hydrocarbon Radicals and Biradicals. J. Phys. Chem. A 2013, *117*, 3697–3717.

[5] See, e.g., the entire special issue of Chem. Rev. 2012, *112*, 1.

[6] Schmatz, S. Approximate Calculation of Anharmonic Densities of Vibrational States for Very Large Molecules. Chem. Phys. 2008, *346*, 198–211.

[7] Troe, J.; Ushakov, V. G. Anharmonic Rovibrational Numbers and Densities of States for HO_2, H_2CO, and H_2O_2. J. Phys. Chem. A 2009, *113*, 3940–3945.

[8] Nguyen, T. L.; Barker, J. R. Sums and Densities of Fully Coupled Anharmonic Vibrational States: A Comparison of Practical Methods. J. Phys. Chem. A 2010, *114*, 3718–3730.

[9] Zheng, J.; Yu, T.; Papajak, E.; Alecu, I. M.; Mielke, S. L.; Truhlar, D. G. Practical Methods for Including Torsional Anharmonicity in Thermochemical Calculations. Phys. Chem. Chem. Phys. 2011, *13*, 10885–10907.

[10] Kamarchik, E.; Jasper, A. W. Anharmonic State Counts and Partition Functions for Molecules via Classical Phase Space Integrals in Curvilinear Coordinates. J. Chem. Phys. 2013, *138*, 194109.

[11] Kamarchik, E.; Jasper, A. W. Anharmonic Vibrational Properties from Intrinsic n-Mode State Densities. J. Phys. Chem. Lett. 2013, *4*, 2430–2435.

[12] Goldsmith, C. F.; Magoon, G. R.; Green, W. H. Database of Small Molecule Thermochemistry for Combustion. J. Phys. Chem. A, 2012, *116*, 9033–9057.

[13] S. J. Klippenstein, L. B. Harding, and B. Ruscic, Ab initio Computations and Active Thermochemical Tables Hand in Hand: Heats of Formation of Core Combustion Species, in preparation (2013).

[14] Fernandez-Ramos, A.; Miller, J. A.; Klippenstein, S. J.; Truhlar, D. G. Modeling the Kinetics of Bimolecular Reactions. Chem. Rev. 2006, *106*, 4518–4584.

[15] Baldridge, K. K.; Gordon, M. S.; Steckler, R.; Truhlar. D. G. An Initio Reaction Paths and Direct Dynamics Calculations. J. Phys. Chem. 1989, *93*, 5107–5119.

[16] Georgievskii, Y.; Miller, J. A.; Klippenstein, S. J. Association Rate Constants for Reactions Between Resonance-Stabilized Radicals: C_3H_3+C_3H_3, C_3H_3+C_3H_5, and C_3H_5+C_3H_5. Phys. Chem. Chem. Phys. 2007, *9*, 4259–4268.

[17] Georgievskii, Y.; Klippenstein, S. J. Variable Reaction Coordinate Transition State Theory: Analytic Results and Application to the C_2H_3+H --> C_2H_4 Reaction. J. Chem. Phys. 2003, *118*, 5442–5455.

[18] Klippenstein, S. J.; Georgievskii, Y.; Harding, L. B. Statistical Theory for the Kinetics and Dynamics of Roaming Reactions. J. Phys. Chem. A, 2011, *115*, 14370–14381.

[19] Tao, Y.; Zheng, J.; Truhlar, D. G. Multipath Variational Transition State Theory: Rate Constant of the 1,4-Hydrogen Shift. J. Phys. Chem. A 2012, *116*, 297–308.

[20] Harding, L. B.; Klippenstein, S. J.; Jasper, A. W. Separability of Tight and Roaming Pathways to Molecular Decomposition. J. Phys. Chem. A 2012, *116*, 6967–6982.

[21] Harding, L. B.; Klippenstein, S. J.; Jasper, A. W. Ab Initio Methods for Reactive Potential Surfaces. Phys. Chem. Chem. Phys. 2007, *9*, 4055–4070.

[22] Dagdigian, P. J.; Alexander, M. H. Exact Quantum Scattering Calculations of Transport Properties: CH_2–He. J. Chem. Phys. 2013, 138, 164305.

[23] Ivanov, M. V.; Babikov, D. Collisional Stabilization of van der Waals States of Ozone. J. Chem. Phys. 2011, *134*, 144107.

[24] Semenov, A.; Babikov, D. Equivalence of the Ehrenfest Theorem and the Fluid-Rotor Model for Mixed Quantum/Classical Theory of Collisional Energy Transfer. J. Chem. Phys. 2013, *138*, 164110.

[25] Brown, N. J.; Miller J. A. Collisional Energy-Transfer in the Low-Pressure-Limit Unimolecular Dissociation of HO_2. J. Chem. Phys. 1984, *80*, 5568–5580.

[26] Lim, K. F.; Gilbert, R. G. Calculation of Collisional-Energy-Transfer Rates in Highly Excited Molecules. J. Phys. Chem. 1990, *94*, 72–77.

[27] Lenzer, T.; Luther, K.; Troe, J; Gilbert, R. G.; Lim, K. F. Trajectory Simulations of Collisional Energy-Transfer in Highly Excited Benzene and Hexafluorobenzene. J. Chem. Phys. 1995, *103*, 626–641.

[28] Meroueh, O.; Hase, W. L. Collisional Activation of Small Peptides. J. Phys. Chem. A 1999, *103*, 3981–3990.

[29] Brunsvold, A. L.; Garton, D. J.; Minton, T. K.; Troya, D.; Schatz, G. C. Crossed Beams and Theoretical Studies of the Dynamics of Hyperthermal Collisions Between Ar and Ethane. J. Chem. Phys. 2004, *121*, 11702–11714.

[30] Oref, I. Israel Collisional Energy Transfer in Polyatomic Molecules in the Gas Phase. J. Chem. 2007, *47*, 205–214.

[31] Barker, J. R.; Weston, R. E. Collisional Energy Transfer Probability Densities P(E, J; E', J') for Monatomics Colliding with Large Molecules. J. Phys. Chem. A, 2010, *114*, 10619–10633; 2012, *116*, 799.

[32] Tardy, D. C.; Rabinovitch, B. S. Collisional Energy Transfer. Thermal Unimolecular Systems in the Low-Pressure Region. J. Chem. Phys. 1966, *45*, 3720–3730.

[33] Tardy, D. C.; Rabinovitch, B. S. Intermolecular Vibrational Energy Transfer in Thermal Unimolecular Systems. Chem. Rev. 1977, *77*, 369–408.

[34] Troe, J. Theory of Thermal Unimolecular Reactions at Low-Pressures. 1. Solutions of the Master Equation. J. Chem. Phys. 1977, *66*, 4745–4757.

[35] Troe, J. Theory of Thermal Unimolecular Reactions at Low-Pressures. 2. Strong Collision Rate Constants – Applications. J. Chem. Phys. 1977, *66*, 4758–4775.

[36] Baer, T.; Hase, W. L. Unimolecular Reaction Dynamics: Theory and Experiments; Oxford Universtiy Press: New York, 1996.

[37] Keck, J.; Carrier, G. Diffusion Theory of Nonequilibrium Dissociation and Recombination. J. Chem. Phys. 1965, *43*, 2284–2298.

[38] Schiff, L. I. Quantum Mechanics, 3rd Edition (McGraw-Hill, New York, 1968), pp. 28–30.

[39] Miller, W. H. Classical S-Matrix for Rotational Excitation: Quenching of Quantum Effects in Molecular Collisions. J. Chem. Phys. 1971, *54*, 5386–5397.

[40] Heller, E. J. Time-Dependent Approach to Semiclassical Dynamics. J. Chem. Phys. 1975, *62*, 1544–1555.

[41] Jasper, A. W.; Miller, J. A. Collisional Energy Transfer in Unimolecular Reactions: Direct Classical Trajectories for $CH_4 \leftrightarrows CH_3 + H$ in Helium. J. Phys. Chem. A 2009, *113*, 5612–5619.

[42] Jasper, A. W.; Miller, J. A. Theoretical Unimolecular Kinetics for $CH_4 + M \leftrightarrows CH_3 + H + M$ in Eight Baths, M = He, Ne, Ar, Kr, H_2, N_2, CO, and CH_4. J. Phys. Chem. A 2011, *115*, 6438–6455.

[43] Smith, S. C.; Gilbert, R. G. Angular-Momentum Conservation in Unimolecular and Recombination Reactions. Int. J. Chem. Kinet. 1988, *20*, 307–329.

[44] Miller, J. A.; Klippenstein, S. J.; Raffy, C. Solution of Some One- and Two-Dimensional Master Equation Models for Thermal Dissociation: The Dissociation of Methane in the Low-Pressure Limit. J. Phys. Chem. A 2002, *106*, 4904–4913.

[45] Troe, J; Ushakov, V. G. The Dissociation/Recombination Reaction CH_4 (+M) $\leftrightarrows$ CH_3+H (+M): A Case Study for Unimolecular Rate Theory. J. Chem. Phys. 2012, *136*, 214309.

[46] Srinivasan, N. K.; Michael, J. V. The Thermal Decomposition of Water. Int. J. Chem. Kinet. 2006, *38*, 211–219.

[47] Michael, J. V.; Su, M.-C.; Sutherland, J. W.; Carroll, J. J.; Wagner, A. F. Rate Constants for $H+O_2+M \leftrightarrows HO_2+M$ in Seven Bath Gases. J. Phys. Chem. A 2002, *106*, 5297–5313.

[48] Fletcher, F. J.; Rabinovitch, B. S.; Watkins, K. W.; Locker, D. J. Energy Transfer in Thermal Methyl Isocynamic Isomerization. Experimental Survey. J. Phys. Chem. 1966, *70*, 2823–2833.

[49] Bunker, D. L.; Jayich, S. A. Trajectory Studies of Energy Transfer: CH_3NC with He, Xe, H_2, and N_2. Chem. Phys. 1976, *13*, 129–134.

[50] Altinay, G.; Macdonald, R. G. Determination of the Rate Constant for the NH_2 + NH_2 Recombination Reaction with Collision Partners He, Ne, Ar, and N_2 at Low Pressures and 296 K. Part 1. J. Phys. Chem. A 2012, *116*, 1353–1367. Altinay, G.; Macdonald, R. G. Determination of the Rate Constants for the NH_2 + NH_2 and NH_2 + H Recombination Reactions with Collision Partners CH_4, C_2H_6, CO_2, CF_4, and SF_6 at Low Pressures and 296 K. Part 2. 2012, *116*, 2161–2176.

[51] Hu, X.; Hase, W. L. Effect of Anharmonicity on Intermolecular Energy-Transfer from Highly Vibrationally Excited Molecules. J. Phys. Chem. 1988, *92*, 4040–4064.

[52] Lim, K. F. Quasi-classical Trajectory Study of Collisional Energy-Transfer in Toluene Systems. 1. Argon Bath Gas – Energy-Dependence and Isotope Effects. J. Chem. Phys. 1994, *100*, 7385–7399.

[53] Lenzer, T.; Luther, K. Intermolecular Potential Effects in Trajectory Calculations of Collisions Between Large Highly Excited Molecules and Noble Gases. J. Chem. Phys. 1996, *105*, 10944–10953.

[54] Yoder, L. M.; Barker, J. R. Quasiclassical Trajectory Simulations of Pyrazine-Argon and Methylpyrazine-Argon van der Waals Cluster Predissociation and Collisional Energy Transfer. J. Phys. Chem. A 2000, *108*, 10184–10193.

[55] Lendvay, G.; Schatz, G. C. Comparison of Master Equation and Trajectory Simulation of the Relaxation of an Ensemble of Highly Vibrationally Excited Molecules. J. Phys. Chem. 1994, *98*, 6530–6536.

[56] Jasper, A. W.; Klippenstein, S. J.; Miller, J. A., unpublished (2013).

[57] Robertson, S. H.; Shushin, A. I.; Wardlaw, D. M. Reduction of the 2-Dimensional Master Equation to a Smoluchowsky Type Differential-Equation with Application to $CH_4 \leftrightarrows CH_3 + H$. J. Chem. Phys. 1993, *98*, 8673–8679.

[58] Jeffrey, S. J.; Gates, K. E.; Smith, S. C. Full Iterative Solution of the Two-Dimensional Master Equation for Thermal Unimolecular Reactions. J. Phys. Chem. 1996, *100*, 7090–7096.

[59] Robertson, S. H.; Pilling, M. J.; Green, N. J. B. Diffusion Approximations of the Two-Dimensional Master Equation. Mol. Phys. 1996, *89*, 1531–1551.

[60] Gordon, M. S.; Truhlar, D. G. Scaling All Correlation-Energy in Perturbation-Theory Calculations of Bond-Energies and Barrier Heights. J. Am. Chem. Soc. 1986, *108*, 5412–5419.

[61] Wang, Y.; Mak, C. H. Transferable Tight-Binding Potential for Hydrocarbons. Chem. Phys. Lett. 1995, *235*, 37–46.

[62] Andersen, H. C. Molecular-Dynamics Simulations at Constant Pressure and/or Temperature. J. Chem. Phys. 1980, *72*, 2348–2393.

[63] Faist, M. B.; Muckerman, J. T.; Schubert, F. E. Importance Sampling and Histogrammic Representations of Reactivity Functions and Product Distributions in Monte-Carlo Quasiclassical Trajectory Calculations. J. Chem. Phys. 1978, *69*, 4087–4096.

[64] Jasper, A. W.; Oana, C. M.; Truhlar, D. G. DiNT: Direct Nonadiabatic Trajectories. A Direct Trajectory Code for Adiabatic and Nonadiabatic Chemistry, July, 2013. <www.sandia.gov/~ajasper/dint>.

[65] Efron, B. 1977 Rietz Lecture: Bootstrap Methods: Another Look at the Jackknife. Ann. Stat. 1979, 7, 1–26.

[66] Nangia, S.; Jasper, A. W.; Miller, III, T. F.; Truhlar, D. G. Army Ants Algorithm for Rare Event Sampling of Delocalized Nonadiabatic Transitions by Trajectory Surface Hopping and the Estimation of Sampling Errors by the Bootstrap Method. J. Chem. Phys. 2004, *120*, 3586–3597.

[67] Jasper, A. W.; Miller, J. A. Lennard-Jones Parameters for Combustion and Chemical Kinetics Modeling from Full-Dimensional Intermolecular Potentials. Combust. Flame, in press (2013). DOI: 10.1016/j.combustflame.2013.08.004

[68] Maergoiz, A. I.; Nikitin, E. E.; Troe, J.; Ushakov, V. G. Classical Trajectory and Adiabatic Channel Study of the Transition From Adiabatic to Sudden Capture Dynamics. III. Dipole-Dipole Capture. J. Chem. Phys. 1996, *105*, 6277.

[69] Fernandes, R. X.; Luther, K.; Troe, J.; Ushakov, V. G. Experimental and Modelling Study of the Recombination Reaction $H + O_2$ (+M) → HO_2 (+M) Between 300 and 900 K, 1.5 and 950 bar, and in the Bath Gases M = He, Ar, and N_2. Phys. Chem. Chem. Phys. 2008, *10*, 4313–4321.

[70] Barker, J. R.; Golden, D. M. Master Equation Analysis of Pressure-Dependent Atmospheric Reactions. Chem. Rev. 2003, *103*, 4577–4591.

[71] Pilling, M. J.; Robertson, S. H. Master Equation Models for Chemical Reactions of Importance in Combustion. Annu. Rev. Phys. Chem. 2003, *54*, 245–275.

[72] Miller, J. A.; Klippenstein, S. J. Master Equation Methods in gas Phase Chemical Kinetics. J. Phys. Chem. A 2006, *110*, 10528–10544.

[73] Gilbert, R. G. Theory of Collisional Energy Transfer of Highly Excited Molecules. Int. Rev. Phys. Chem. 1991, *10*, 319–347.

[74] Strekalov, M. L. Collisional Energy Transfer of Highly Excited Polyatomic Molecules as a Stochastic Process. Chem. Phys. 2011, *389*, 47–52.

[75] Miller, J. A.; Klippenstein, S. J. The H+C_2H_2 (+M) ⇆ C_2H_3 (+M) and H+C_2H_2 (+M) C2H5 ⇆ (+M) Reactions: Electronic Structure, Variational Transition-State Theory, and Solutions to a Two-Dimensional Master Equation. Phys. Chem. Chem. Phys. 2004, *6*, 1192–1202.

[76] Klippenstein, S. J.; Miller, J. A. The Addition of Hydrogen Atoms to Diacetylene and the Heats of Formation of i-C_4H_3 and n-C_4H_3. J. Phys. Chem. A 2005, *109*, 4285–4295.

[77] Senosiain, J. P.; Klippenstein, S. J.; Miller, J. A. The Reaction of Acetylene with Hydroxyl Radicals. J. Phys. Chem. A 2005, *109*, 6045–6055.

[78] Sellevåg, S. R.; Georgievskii, Y.; Miller, J. A. The Temperature and Pressure Dependence of the Reactions H+O_2(+M) ⇆ HO_2(+M) and H+OH(+M) ⇆ H_2O(+M). J. Phys. Chem. A 2008, *112*, 5085–5095.

[79] Miller, J. A.; Klippenstein, S. J. Dissociation of Propyl Radicals and Other Reactions on a C3H7 Potential. J. Phys. Chem. A 2013, *117*, 2718–2727.

[80] Clarke, D. L.; Thompson, K. C.; Gilbert, R. G. Supercollision Events in Weak Collisional Energy-Transfer of Highly Excited Species. Chem. Phys. Lett. 1991, *182*, 357–362.

[81] Bernshtein, V.; Oref, I.; Lendvay, G. Energy Transfer Rate Coefficients from Trajectory Calculations and Contributions of Supercollisions to Reactive Rate Coefficients. J. Phys. Chem. 1996, *100*, 9738–9744.

[82] Liu, C.-L.; Hsu, H. C.; Lyu, J.-J.; Ni, C.-K. Supercollisions and Energy Transfer of Highly Vibrationally Excited Molecules. J. Chem. Phys. 2005, *123*, 131102.

[83] Gilbert, R. G. Collisional Energy Exchange in Highly Vibrationally Excited Molecules: The Biased Random Walk Model. J. Chem. Phys. 1984, *80*, 5501–5509.

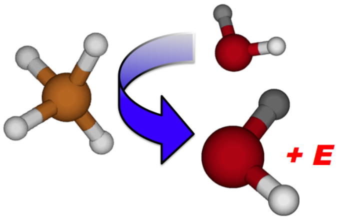ToC Graphic